

Received June 6, 2019, accepted June 16, 2019, date of publication June 24, 2019, date of current version July 11, 2019.

Digital Object Identifier 10.1109/ACCESS.2019.2924522

Performance Analysis of Cognitive Clustered M2M Random Networks With Joint User and Machine Device Selection

MOHAMMED A. M. ABDULLAH¹, (Member, IEEE), ZAID ABDULLAH², (Member, IEEE),
GAOJIE CHEN², (Senior Member, IEEE), JIE TANG³, (Senior Member, IEEE),
AND JONATHON CHAMBERS², (Fellow, IEEE)

¹Computer and Information Engineering Department, College of Electronics Engineering, Ninevah University, Mosul 41002, Iraq

²Department of Engineering, University of Leicester, Leicester LE1 7HB, U.K.

³School of Electronic and Information Engineering, South China University of Technology, Guangzhou 510006, China

Corresponding author: Gaojie Chen (gaojie.chen@leicester.ac.uk)

This work was supported by the EPSRC under Grant EP/R006377/1 (communications signal processing-based solutions for massive machine-to-machine networks (M3NETs)).

ABSTRACT In this paper, a machine-to-machine (M2M) communication system is proposed with joint M2M and cellular user equipment (CUE) device selection schemes to decrease the outage probability of the system. The machine devices and CUEs are positioned randomly according to a binomial point process (BPP), and two novel ordering metrics are proposed for the joint selection scheme: one based on the locations of the M2M devices and the other based on instantaneous channel gains. The simulation results confirm that the proposed selection scheme attains a significant reduction in the outage probability for M2M networks while limiting the interference to the base station (BS) by a delimited threshold. A hybrid-duplex BS is employed to switch between a half-duplex (HD) and a full-duplex (FD) to attain the best performance corresponding to various levels of residual self-interference. The closed-form formulas of the outage probability are derived for each of these ordering policies corresponding to different path loss exponents, and the analytical results are verified through Monte Carlo simulations. The proposed model and its related analysis is given in this paper lead the way for further work in the 5G Internet of Things (IoT) area.

INDEX TERMS M2M communications, stochastic geometry, cognitive radio, hybrid-duplex, device selection.

I. INTRODUCTION

The Internet of Things (IoT) promises to provide contemporary administrations for a wide scope of application, extending from individual to industrial environments [1]. Machine-to-Machine (M2M) networks is a special case of the IoT which provide the IoT with the connectivity. In the near future, M2M communications are anticipated to be broadly utilized in different applications [2], [3], including health-care, smart meters, cloud computing, traffic control and monitoring of agricultural and industrial applications [4].

The number of Machine-to-Machine devices are increasing exponentially, and according to Ericson [5], is predicted to reach multi-billion by next year. Unfortunately, this expanding number of M2M devices has many consequences

including interference, high power consumption, and spectrum scarcity [6], [7].

To unleash the potential of the M2M paradigm and address the aforementioned spectrum scarcity in M2M networks [8], Cognitive Radio (CR) [9] can be integrated with M2M communications resulting in the term *cognitive M2M communications*. CR technology can boost the spectrum by sharing resources between the primary and secondary users [10]. Spectrum sharing schemes include underlay, overlay and interweave, and among them, the underlay scheme is favorable in M2M networks due to its high spectral and power efficiency with low delay in transmission [11]. In the underlay scheme, the spectrum of the primary user can only be accessed by the secondary user if the interference is below a certain level.

Generally speaking, in a metropolitan area, M2M devices are adjacent to each other [12]. Driven by this topology,

The associate editor coordinating the review of this manuscript and approving it for publication was Hayder Al-Hraishawi.

we therefore propose a system model exploiting cluster-based M2M communications where the cluster head collects the traffic from M2M devices using CR technology. Therefore, in this scheme, the cluster-head acts as a gateway for the M2M devices to access the BS and hence reduces the number of direct access to the BS. Consequently, the probability of collision is decreased and the congestion problem of M2M devices is alleviated [13].

In the literature, the work on M2M communications is in early stages with only limited works focusing on cognitive or cluster-based M2M scenarios. In this context, a cluster-based scheme is presented by Wang *et al.* [14] where M2M traffic is directed to the BS under the control of the cluster-head while the Cellular User Equipment (CUE) devices can directly access the BS. The proposed model is analyzed with respect to the Random Access CHannel (RACH). A cluster-based approach is introduced by Jung *et al.* [15] to decrease M2M traffic in a cellular network. In their proposed system, it is assumed that M2M devices can communicate with each other using a local network. On the other hand, M2M devices can access the BS using a cellular radio by selecting a group leader. Lee *et al.* [8] proposed a cluster-based M2M architecture solve the RACH problem of M2M over cellular networks. In this scenario, M2M devices can access the BS either indirectly via a cluster-head utilizing CR technology or directly over a cellular network. The authors reported an improvement in the performance using this scenario where the number of direct access to the BS is decreased.

Despite that the previous works employed a cluster-based approach for M2M networks, these works are still in infancy reporting only prototypes with limited corresponding analysis or theoretical realizations. In our previous work [16], we proposed a cluster-based architecture for M2M communications utilizing underlay CR approach. We also proposed a joint selection scheme for CUE and M2M devices to decrease the outage probability of M2M networks. Although the proposed scheme showed a significant improvement in the outage probability, the applicability of the proposed scheme is limited in real-life scenarios as the M2M and CUE devices are assumed to be stationary. This paper addresses the aforementioned drawbacks by employing stochastic geometry to simulate the mobile nature of M2M and CUEs devices.

Stochastic geometry is a powerful tool to model and analyze wireless networks assuming that the locations of nodes are random due to their unpredictable spatial characteristics [17]–[19]. We adopt stochastic geometry to model and analyze our system assuming nodes with random locations. The CUEs and M2M devices have unpredictable spatial characteristics which can be simulated using a random point pattern or a point process. These include, but are not limited to Binomial Point Process (BPP) and Poisson Point Process (PPP). PPP has been widely used to model large-scale random networks due to its simplicity. However, it cannot be used to model finite network with a given number of nodes [20]. Moreover, when the number of nodes is small, the PPP model is inaccurate [21]. Therefore, the BPP model suits M2M

networks due to the finite number of M2M devices inside each cluster and hence it has been adopted in our work. Stochastic geometry is particularly useful in large M2M networks as it is almost impossible for a node to have knowledge of the locations of other nodes apart from the adjacent nodes. Although M2M devices are in general stationary, but for different time-slots, M2M devices can be active or silent. This is equivalent to randomly located M2M devices when the density of M2M devices is large. In addition, some emerging applications employing M2M do require moving devices. This falls in the new area of moving IoT such as robotics and smart vehicles or those devices that require a mobile nature such as wearable devices including smartwatches and fitness trackers [22], [23]. In this case stochastic geometry for M2M is a necessity.

Despite stochastic geometry being widely used in large scale ad-hoc and cellular wireless networks [24], [25], only a few papers employ stochastic geometry in the context of M2M communications [26]–[28], as the vast majority of work in M2M communications assume a fixed topology and ignore the outage characteristics for each link, which is unrealistic in a large network. To this end, most of the works that adopt stochastic geometry focus on power consumption in M2M networks. For example, Malak *et al.* [26] proposed a multi-hop data aggregation scheme to minimize the average total energy consumption of an M2M network, where stochastic geometry was employed to incorporate the coverage characteristics for different transmission modes. Kouzayha *et al.* [27] applied stochastic geometry to model and analyze the performance of an M2M network under a power saving scheme, which triggers the devices when there is a need for certain sensing or communications activity. Swain *et al.* [28] proposed a framework to analyze the impact of multi-hop Device-to-Device (D2D) communication in increasing the network coverage and average rate of an M2M device with the help of stochastic geometry. It can be seen from the above that there is a gap in the literature in terms of employing stochastic geometry with M2M networks. Therefore, this work attempts to bridge the gap in this field.

This work is amongst the first in the literature which derives closed-form expressions for the outage probability of the proposed M2M model using the stochastic geometry approach. In addition, we propose and analyze the performance of two novel ordering approaches for M2M networks: one based on instantaneous Channel State Information (CSI), and one based on large-scale fading. The contributions of this paper, which to the best of our knowledge have not been considered in any previously published work, can be summarized as follows:

- We propose a new cognitive cluster-based M2M system, where stochastic geometry is adopted to model the locations of the CUEs and M2M devices.
- Two novel policies for joint CUE and M2M devices selection are proposed to maximize the Signal to Interference Ratio (SIR), where the first policy depends on the locations of the M2M devices, while

TABLE 1. Notation and symbols used in the paper.

Symbol	Definition/Explanation
AWGN	Additive White Gaussian Noise
BS	Base Station
BPP	Binomial Point Process
CSI	Channel State Information
CR	Cognitive Radio
CUE	Cellular User Equipment
DF	Decode-and-Forward
FD	Full-Duplex
HD	Half-Duplex
SIR	Signal-to-Interference Ratio
I_{th}	interference threshold
K	the number of M2M devices
L	the number of CUEs
m_i	the i^{th} M2M device
CUE_j	the j^{th} CUE
$E[\cdot]$	the expectation operator
$\ln(\cdot)$	natural logarithm
α	path loss exponent
$\mathbb{P}(\cdot)$	Probability operator
$\beta(\cdot)$	Beta function
$\text{erf}(\cdot)$	error function
$\text{erfc}(\cdot)$	complementary error function
$\Gamma(\cdot)$	Gamma function
$\mathcal{HG}(\cdot)$	Hyper Geometric function
$Ei(1, a)$	Exponential integral function
$\mathcal{MG}(\cdot)$	Meijer's G function
$\mathcal{WK}(\cdot)$	Whittaker function

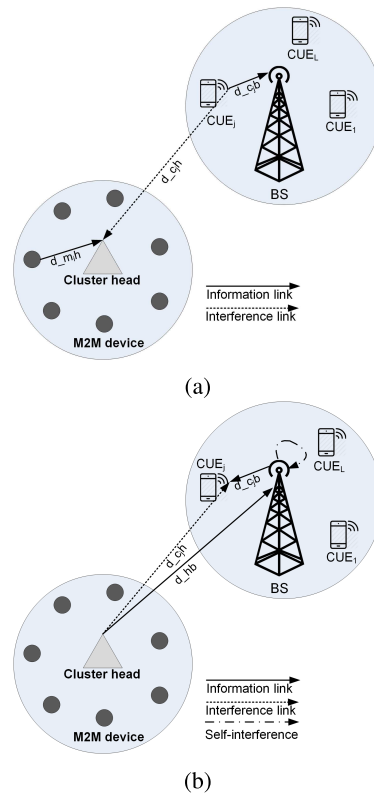


FIGURE 1. System model of the proposed scheme with a cluster-head, L CUEs, and K M2M devices: (a) First-hop (T_1) and (b) second-hop (T_2).

the second one depends on the instantaneous channel gains.

- Closed-form expressions for the outage probability are derived for the proposed system model for both selection methods, and for different values of path loss exponent, which verified through Monte Carlo simulations.

This paper is organized as follows. Section II introduces the system model while Section III presents the outage probability analysis. The simulation results and their corresponding analysis are presented in Section IV. Finally, Section V concludes this paper. Table 1 shows the notation symbol used in this paper.

II. SYSTEM MODEL

Fig. 1 depicts the proposed system model where there is one BS with hybrid-duplex antenna [14], L single-antenna CUEs,¹ and K single-antenna M2M devices, which are randomly located inside a cluster with a radius of R_m . The communication of M2M devices is controlled by a cluster-head [8], which is assumed to be a Decode-and-Forward (DF) relay [29] to decode and forward the information from the M2M device to the BS. In our system, it is assumed that a CUE device can access the channel using TDMA, and one M2M device shares the same spectrum with the CUE. The selection policies for the CUE and M2M device will be explained in section III.

¹The CUEs are randomly located inside a cluster with a radius of R_c , which can guarantee a reliable communication with the BS.

The proposed scheme is designed to work in two hops: In the first-hop (T_1), the cluster-head collects data from an M2M device and the BS works in Half-Duplex (HD) mode to receive data from a CUE as illustrated in Fig. 1(a). In the second-hop (T_2), the BS operates in Full-Duplex (FD) mode to send data to a CUE and receive data from the cluster-head at the same time, as shown in Fig. 1(b).

Without loss of generality, we assume the BS is located at the origin of a 2-dimensional Euclidean space \mathbb{R}^2 , and the cluster-head is located at a fixed point. The locations of the M2M devices and CUEs are uniformly distributed according to a spatial BPP denoted by Φ_M and Φ_C , respectively. The small-scale fading channels $machine_i \rightarrow cluster - head$, $cluster - head \rightarrow BS$, $cluster - head \rightarrow CUE_j$, $CUE_j \rightarrow BS$, and $BS \rightarrow CUE_j$, which are denoted as $h_{m,h}$, h_{hb} , h_{hc_j} , $h_{c_j,b}$, and h_{bc_j} respectively, are independent² and identically distributed (i.i.d.) random variables. Hence, the channel coefficient between nodes i and j , taking into account both small and large scale fading coefficients, and can be decomposed as $g_{ij} = h_{ij}d_{ij}^{-\alpha/2}$, where d_{ij} and α denote the distance between the two nodes and the path loss exponent, respectively.

The small-scale fading coefficients h_{ij} are modeled as zero-mean Rayleigh fading channels with unit variance. Therefore,

² $h_{c_j,b}$ and h_{bc_j} are independent because they took place at two different hops.

the corresponding channel gains $\gamma_{ij} = |h_{ij}|^2$ are independently and exponentially distributed with mean value λ_{ij} [30]. Due to the Quasi-static channels assumption, the channel coefficients independently vary from one coherence time interval to another but remain unchanged within one packet duration [31]. As the underlay scenario is exploited in our model, therefore, the maximum transmit power of the cluster-head³ is restrained in order to detain any harmful interference to the CUE_j [29], and can be defined as $P_h \leq \frac{I_h d_{cjh}^\alpha}{|h_{cjh}|^2}$ where I_h is the interference threshold. No power constraint is imposed on the M2M devices because they do not hinder the BS due to the limited power needed for an M2M device to transmit to the cluster-head as they are contained within the same cluster [13], [34]. In the next section, the proposed ordering policies will be introduced and the two-hops system will be analyzed.

III. PERFORMANCE ANALYSIS OF THE PROPOSED TWO-HOPS SYSTEM

In this section, we derive closed-form expressions for the outage probability of our proposed two-hops system with joint CUE and M2M device selection.

A. FIRST-HOP (T_1)

In the first hop, we propose two novel policies for the joint CUE and M2M device selection to maximize the SIR at the cluster-head. The two selection methods are explained alongside their analysis in the following subsections.

1) POLICY I: ORDERING BY INSTANTANEOUS CHANNEL GAINS

In the first-hop, an M2M device m_i transmits its signal x_{m_i} , with $|x_{m_i}|^2 = 1$, to the cluster-head sharing uplink radio resource with the CUE. Hence, the received signal at the cluster-head can be obtained as

$$y_h = \frac{\sqrt{P_{m_i}} h_{m_i h} x_{m_i}}{d_{m_i h}^{\alpha/2}} + \frac{\sqrt{P_{c_j}} h_{c_j h} x_{c_j}}{d_{c_j h}^{\alpha/2}} + n_h, \quad (1)$$

where P_{m_i} and P_{c_j} denote the transmit powers of m_i and CUE_j, respectively; x_{c_j} is the interference signal sent from CUE_j, with $|x_{c_j}|^2 = 1$, $d_{m_i h}$ denotes the distance between m_i and the cluster-head, $d_{c_j h}$ is the distance between CUE_j and the cluster-head and n_h is the AWGN at the cluster-head with zero mean and variance of σ_h^2 . We assume $P_{m_i} = P_m \forall i \in \{1 \dots K\}$; $P_{c_j} = P_c \forall j \in \{1 \dots L\}$. The distance between a CUE_j and the cluster-head can be calculated as $d_{c_j h} = \sqrt{d_{c_j b}^2 + d_{hb}^2 - 2 \cos(\theta) d_{c_j b} d_{hb}}$ where $d_{c_j b}$ is the distance between CUE_j and the BS, d_{hb} is a fixed distance between the cluster-head and the BS, and θ is the angle between the cluster-head and CUE_j at the BS. When $d_{hb} \gg d_{c_j b}$, $d_{c_j h} \approx d_{hb}$. This is because the CUEs are usually located

³The CSI between the cluster-head and the CUE is usually estimated through pilots and feedback (e.g. [32]), and the CSI estimation without feedback may also be applied (e.g [33]). The detail of the channel estimation is beyond the scope of this paper.

close to the BS while the cluster-head is based far away from the BS. In the interference limited scenario, the instantaneous SIR at the cluster-head can be derived from (1) as:

$$\gamma_h = \frac{\frac{P_m |h_{m_i h}|^2}{d_{m_i h}^\alpha}}{\frac{P_c |h_{c_j h}|^2}{d_{c_j h}^\alpha} + \sigma_h^2} \approx \frac{\frac{P_m |h_{m_i h}|^2}{d_{m_i h}^\alpha}}{\frac{P_c |h_{c_j h}|^2}{d_{hb}^\alpha}}. \quad (2)$$

To maximize the SIR, the joint selection of CUE and M2M device can be expressed as follows:

$$\gamma_{T_1}^1 = \frac{\max_{i \in \{1 \dots K\}} \left(\frac{P_m |h_{m_i h}|^2}{d_{m_i h}^\alpha} \right)}{\min_{j \in \{1 \dots L\}} \left(\frac{P_c |h_{c_j h}|^2}{d_{hb}^\alpha} \right)}. \quad (3)$$

To derive a closed form expression for the CDF of (3), we let $Y_i = \max_{i \in \{1 \dots K\}} \left(\frac{P_m |h_{m_i h}|^2}{d_{m_i h}^\alpha} \right)$ and $X_j = \min_{j \in \{1 \dots L\}} \left(\frac{P_c |h_{c_j h}|^2}{d_{hb}^\alpha} \right)$. When $\alpha = 2$, the CDF of Y_i can be calculated as:

$$\begin{aligned} F_Y(y) &= \mathbb{P} \left(\max_{i \in \{1 \dots K\}} \left(\frac{P_m |h_{m_i h}|^2}{d_{m_i h}^2} \right) < y \right) \\ &\stackrel{a}{=} E \left[\prod_{i \in \{1 \dots K\}} \mathbb{P}(P_m |h_{m_i h}|^2 < y d_{m_i h}^2) \right] \\ &= E_{\Phi_M} \left[\prod_{i \in \{1 \dots K\}} \left(1 - e^{-\frac{y r^2}{P_m}} \right) \right] \\ &\stackrel{b}{=} \left(\frac{1}{\pi R_m^2} \int_0^{R_m} r \left(1 - e^{-\frac{y r^2}{P_m}} \right) dr \right)^K \\ &\stackrel{c}{=} \left(1 - \frac{(1 - e^{-\frac{R_m^2 y}{P_m}}) P_m}{y R_m^2} \right)^K, \end{aligned} \quad (4)$$

where (a) follows from the independence of the random variables $\{|h_{m_i h}|^2; \forall i \in \{1 \dots K\}\}$, (b) holds by using the probability generating functional (PGFL) metric [35], and (c) holds by using (3.321.4) in [36].

The CDF of the denominator in (3) can be calculated as [37]:

$$\begin{aligned} F_X(x) &= 1 - \mathbb{P} \left(\min_{j \in \{1 \dots L\}} (X_j) \geq x \right) \\ &= 1 - \prod_{j \in \{1 \dots L\}} \mathbb{P}(X_j \geq x) \\ &= 1 - \prod_{j \in \{1 \dots L\}} \left(1 - \mathbb{P}(X_j) < x \right) \\ &= 1 - \prod_{j \in \{1 \dots L\}} \left(1 - \mathbb{P} \left(\frac{P_c |h_{c_j h}|^2}{d_{hb}^2} < x \right) \right) \\ &\stackrel{a}{=} 1 - E \left[\prod_{j \in \{1 \dots L\}} 1 - \mathbb{P}(P_c |h_{c_j h}|^2 < x d_{hb}^2) \right] \end{aligned}$$

$$F_{\gamma_{T_1}^1}(t_1) = \left\{ \begin{array}{l} \frac{1}{R_m^4 t_1^3 P_c^2} 2d_{hb}^2 LP_m \ln(d_{hb}) + d_{hb}^2 LP_m \ln(L) - d_{hb}^2 LP_m \ln(Ld_{hb}^2 P_m + R_m^2 t_1 P_c) \\ + d_{hb}^2 LP_m \ln(P_m) + P_c R_m^2 t_1, \quad K = 1, \\ \frac{1}{R_m^4 t_1^3 P_c^2} (L^2 d_{hb}^4 P_m^2 \ln(L) - 2L^2 d_{hb}^4 P_m^2 \ln(Ld_{hb}^2 P_m + R_m^2 t_1 P_c) \\ + L^2 d_{hb}^4 P_m^2 \ln(P_m) L^2 d_{hb}^4 P_m^2 \ln(Ld_{hb}^2 P_m + 2R_m^2 t_1 P_c) + 2L^2 d_{hb}^4 P_m^2 \ln(d_{hb}) \\ + 2P_m R_m^2 t_1 d_{hb}^2 LP_c \ln(L) - 4P_m R_m^2 t_1 d_{hb}^2 LP_c \ln(Ld_{hb}^2 P_m + R_m^2 t_1 P_c) \\ + 2P_m R_m^2 t_1 d_{hb}^2 LP_c \ln(P_m) + 2P_m R_m^2 t_1 d_{hb}^2 LP_c \ln(Ld_{hb}^2 P_m + 2R_m^2 t_1 P_c) + \\ 4P_m R_m^2 t_1 d_{hb}^2 LP_c \ln(d_{hb}) + R_m^4 t_1^2 P_c^2, \quad K = 2, \\ \frac{1}{2R_m^6 t^3 P_c^3} (3L^3 d_{hb}^6 P_m^3 + 18L^2 R_m^2 d_{hb}^4 t P_c P_m^2 + 24LR_m^4 d_{hb}^2 t^2 P_c^2 P_m) \ln(Ld_{hb}^2 P_m + 2R_m^2 t P_c) \\ - Ld_{hb}^2 P_m (Ld_{hb}^2 P_m + 3R_m^2 t P_c)^2 \ln(Ld_{hb}^2 P_m + 3R_m^2 t P_c) - \\ 3Ld_{hb}^2 P_m (L^2 d_{hb}^4 P_m^2 + 6LR_m^2 d_{hb}^2 t P_c P_m + 7R_m^4 t^2 P_c^2) \ln(Ld_{hb}^2 P_m + R_m^2 t P_c) + Ld_{hb}^2 P_m (L^2 d_{hb}^4 P_m^2 \\ + 6LR_m^2 d_{hb}^2 t P_c P_m + 6R_m^4 t^2 P_c^2) \ln(P_m) + \\ 2Ld_{hb}^2 P_m (L^2 d_{hb}^4 P_m^2 + 6LR_m^2 d_{hb}^2 t P_c P_m + 6R_m^4 t^2 P_c^2) \ln(d_{hb}) + Ld_{hb}^2 P_m (L^2 d_{hb}^4 P_m^2 \\ + 6LR_m^2 d_{hb}^2 t P_c P_m + 6R_m^4 t^2 P_c^2) \ln(L) + 2R_m^6 t^3 P_c^3, \quad K = 3. \end{array} \right. \quad (7)$$

$$= 1 - E_{\Phi_C} \left[\prod_{j \in \{1 \dots L\}} \left(1 - \left(1 - e^{-\frac{x d_{hb}^2}{P_c}} \right) \right) \right] \stackrel{c}{=} \left(1 - \frac{\sqrt{P_m} \sqrt{\pi} \left(1 - e^{-\frac{-1.095 \sqrt{R_m^2} - 0.756 \gamma_{T_1}^4}{P_m}} \right)}{2\sqrt{y} R_m^2} \right)^K$$

$$\stackrel{b}{=} 1 - \left(\frac{1}{\pi R_c^2} \int_0^{R_c} \left(1 + e^{-\frac{x d_{hb}^2}{P_c}} \right) dr \right)^L$$

$$= 1 - e^{-\frac{x L d_{hb}^2}{P_c}}, \quad (5)$$

where (a) follows from the independence of the random variables $\{|h_{c_j h}|^2; \forall j \in \{1 \dots L\}\}$, and (b) holds by using the PGFL metric. Then, the final expression of $\gamma_{T_1}^1$ when $\alpha = 2$ can be obtained from (4) and (5) as:

$$F_{\gamma_{T_1}^1}(t_1) = \int_0^\infty d_{hb}^2 L e^{\frac{t_1 z d_{hb}^2 L}{P_c}} \left(1 - \frac{(1 - e^{-\frac{R_m^2 t_1 z}{P_m}}) P_m}{t_1 z R_m^2} \right)^K dz. \quad (6)$$

The closed-form solutions for $F_{\gamma_{T_1}^1}$ when $K = 1, K = 2$ and $K = 3$ are given in (7), as shown at the top of the next page.

Similarly, when $\alpha = 4$, the CDF of Y can be calculated as:

$$F_Y(y) = \mathbb{P} \left(\max_{j \in \{1 \dots K\}} \left(\frac{P_m |h_{m_i h}|^2}{d_{m_i h}^4} \right) < y \right)$$

$$\stackrel{a}{=} E \left[\prod_{i \in \{1 \dots K\}} \mathbb{P}(P_m |h_{m_i h}|^2 < y d_{m_i h}^4) \right]$$

$$= E_{\Phi_M} \left[\prod_{i \in \{1 \dots K\}} \left(1 - e^{-\frac{y r^4}{P_m}} \right) \right]$$

$$\stackrel{b}{=} \left(\frac{1}{\pi R_m^2} \int_0^{R_m} r \left(1 - e^{-\frac{y r^4}{P_m}} \right) dr \right)^K$$

$$= \left(1 - \frac{\sqrt{P_m} \sqrt{\pi} \operatorname{erf} \left(\frac{y \sqrt{\pi} R_m^2}{\sqrt{P_m}} \right)}{2\sqrt{y} R_m^2} \right)^K$$

where $\operatorname{erf}(\cdot)$ denotes the error function, (a) follows from the independence of the random variables $\{|h_{m_i h}|^2; \forall i \in \{1 \dots K\}\}$, (b) holds by using the PGFL metric and (c) holds from $\operatorname{erf}(\cdot)$ approximation in [38] as shown $\operatorname{erf}(\cdot) = 1 - e^{-1.095x - 0.7565x^2}$. Then, the final expression of $F_{\gamma_{T_1}^1}$ when $\alpha = 4$ can be obtained as

$$F_{\gamma_{T_1}^1}(t_1) = \int_0^\infty \frac{L d_{hb}^4 e^{-\frac{L d_{hb}^4 z}{P_c}}}{P_c} \times \left(1 - \frac{1}{2} \frac{\sqrt{P_m} \sqrt{\pi} \left(1 - e^{-\frac{-1.095 \sqrt{t_1 z} R_m^2}{P_m} - \frac{0.756 t_1 z R_m^4}{P_m}} \right)}{\sqrt{t_1 z} R_m^2} \right)^K dz. \quad (9)$$

The integral form in (9) can easily be evaluated numerically using standard software packages.

2) POLICY II: ORDERING BY DISTANCE

For this policy, the ordering is based on the distance between m_i and the cluster-head ($d_{m_i h}$). This scenario corresponds to the large-scale fading case which can be written as [39]:

$$\gamma_{T_1}^2 = \frac{P_m |h_{m_i h}|^2}{\frac{\min_{i \in \{1 \dots K\}} (d_{m_i h}^\alpha)}{P_c |h_{c_j h}|^2} \max_{j \in \{1 \dots L\}} (d_{c_j h}^\alpha)}. \quad (10)$$

By letting $U_1 = \frac{P_m |h_{m_i h}|^2}{d_{m_i h}^\alpha}$ and $V_1 = \frac{P_c |h_{c_j h}|^2}{d_{c_j h}^\alpha}$, the CDF of U_1 is $F_{U_1}(u_1 | d_{m_i h}) = 1 - e^{-\frac{u_1 d_{m_i h}^\alpha}{P_m}}$ and the CDF of V_1 is

$F_{V_1}(v_1|d_{cjh}) = 1 - e^{-\frac{v_1 d_{cjh}^\alpha}{P_c}}$. In a 2-dimensional point process ball consisting of K points which are uniformly and randomly distributed inside a ball with radius R centered at the origin o , the Euclidean distance R_k from the origin to its k^{th} nearest point follows a generalized beta distribution, for $r \in [0, R]$ and $k \in [1, K]$ [21]:

$$f_{R_k}(r) = \frac{2\Gamma(k + \frac{1}{2})\Gamma(K + 1)}{R\Gamma(k)\Gamma(K + \frac{3}{2})} \times \beta\left(\frac{r^2}{R^2}; k + \frac{1}{2}, K - k + 1\right). \quad (11)$$

where $\beta(\cdot)$ and $\Gamma(\cdot)$ are the Beta density and Gamma functions, respectively. Following (11) and by letting $r = d_{mh}$, the CDF of U_1 for any value of k in Φ_M when $\alpha = 4$ can be derived as:

$$\begin{aligned} F_{U_1}(u_1) &= \int_0^{R_m} F_{U_1}(u_1|r)f_{R_k}(r)dr \\ &= \frac{\Gamma(k + \frac{1}{2})\Gamma(K - k + 1)}{\beta(k + \frac{1}{2}, K - k + 1)\Gamma(K + \frac{3}{2})} \\ &\quad \times \mathcal{HG}\left(1 - \left[\frac{1}{2}k, \frac{1}{2} + \frac{1}{2}k\right], \left[1 + \frac{1}{2}K, \frac{1}{2} + \frac{1}{2}K\right], \frac{u_1 R_m^4}{P_m}\right), \end{aligned} \quad (12)$$

where $\mathcal{HG}(\cdot)$ denotes the hypergeometric function. Similarly, the CDF of V_1 for any value of k in Φ_C can be calculated as:

$$\begin{aligned} F_{V_1}(v_1) &= \int_0^{R_c} F_{V_1}(v_1|r)f_{R_k}(r)dr \\ &= \frac{\Gamma(L - k + 1)\Gamma(k + \frac{1}{2})\left(1 - e^{-\frac{v_1 d_{hb}^4}{P_c}}\right)}{\beta(k + \frac{1}{2}, L - k + 1)\Gamma(L + \frac{3}{2})}. \end{aligned} \quad (13)$$

Following (12) and (13), the closed form expression for the CDF of $\gamma_{T_1}^2$ for any k when $\alpha = 4$ can be calculated from

(12) and (13) and by using (7.521) in [36] as given in (14), as shown at the top of the next page.

Similarly, the expression for the CDF of $\gamma_{T_1}^2$ for any k when $\alpha = 2$ can be derived as:

$$\begin{aligned} F_{\gamma_{T_1}^2}(t_1) &= \int_0^\infty \frac{\Gamma(K)d_{hb}^2 e^{-\frac{t_1 z d_{hb}^2}{P_c}} \sqrt{\pi}(K(t_1 z)^{-\frac{K}{2}}(-\frac{1}{P_m})^{\frac{1}{2N}} R_m^{-K} e^{-\frac{t_1 z R_m^2}{2P_m}})}{2t_1 z R_m^2 (K + 1)\beta(3/2, K)\Gamma(K + 3/2)P_c} \\ &\quad \times \mathcal{WK}\left(-\frac{K}{2}, \frac{K}{2} + \frac{1}{2}, \frac{t_1 z R_m^2}{P_m}\right) P_m \\ &\quad - t_1 z R^2 K + (t_1 z)^{-\frac{K}{2}} \left(\frac{1}{P_m}\right)^{-\frac{K}{2}} R^{-K} e^{\frac{t_1 z R_m^2}{2P_m}} \\ &\quad \times \mathcal{WK}\left(-\frac{K}{2} + 1, \frac{K}{2} + \frac{1}{2}, \frac{t_1 z R_m^2}{P_m}\right) - t_1 z R^2 dt_1, \end{aligned} \quad (15)$$

where $\mathcal{WK}(\cdot)$ is the Whittaker function [40]. Then, the closed-form solutions for $F_{\gamma_{T_1}^2}$ when $K = 1, K = 2$ and $K = 3$ are given in(16), as shown at the bottom of this page.

For the special case, the CDF of the nearest M2M can be derived by setting $k = 1$ in (12) as:

$$\begin{aligned} F_{M2M_{near}}(u_1) &= \int_0^{R_m} F_{U_1}(u_1|d_{mh})f_{R_1}(r)dr \\ &= 1 - \mathcal{HG}\left(\left[\frac{1}{2}, 1\right], \left[1 + \frac{1}{2}K, \frac{1}{2}K + \frac{1}{2}\right], \frac{-u_1 R_m^4}{P_m}\right). \end{aligned} \quad (17)$$

Finally, the outage probability of $\gamma_{T_1}^{(2)}$ for the nearest M2M device and farthest CUE device can be expressed as:

$$\begin{aligned} F_{\gamma_{T_1}^2}(t_3) &= \int_0^\infty \int_0^{t_3 v_1} f_{M2M}(u_1|d_{mh})f_{CUE}(v_1|d_{hb})du_1 dv_1 \\ &= \frac{2\Gamma(2 + K)\sqrt{2}}{2^{\frac{3}{2}+K}(K + 1)} \end{aligned}$$

$$\begin{aligned} F_{\gamma_{T_1}^2}(t_1) &= \int_0^\infty \int_0^{t_1 v_1} f_{U_1}(u_1)f_{V_1}(v_1)du_1 dv_1 \\ &= \frac{\Gamma(k + 1)\Gamma(K - k + 1)}{\beta(k + \frac{1}{2}, K - k + 1)} \left(1 - \mathcal{HG}\left(\left[1, \frac{1}{2}k, \frac{1}{2} + \frac{1}{2}k\right], \left[1 + \frac{1}{2}K, \frac{1}{2} + \frac{1}{2}K\right], -\frac{t_1 R_m^4 P_c}{P_m d_{hb}^4 \Gamma(K + \frac{3}{2})}\right)\right). \end{aligned} \quad (14)$$

$$F_{\gamma_{T_1}^2}(t_1) = \left\{ \begin{aligned} &\frac{2d_{hb}^2 P_m \ln(d_{hb}) - d_{hb}^2 P_m \ln(R_m^2 t_1 P_c + d_{hb}^2 P_m) + d_{hb}^2 P_m \ln(P_m) + R_m^2 t_1 P_c}{R_m^2 t_1 P_c}, & K = 1, \\ &\frac{1}{t_1^2 R_m^4 P_c^2} (4P_m t R_m^2 d_{hb}^2 P_c \ln(d_{hb}) - 2P_m t R_m^2 d_{hb}^2 P_c \ln(R_m^2 t P_c + d_{hb}^2 P_m) + 2P_m t R_m^2 d_{hb}^2 P_c \ln(P_m) \\ &\quad + t^2 R_m^4 P_c^2 + 4d_{hb}^4 P_m^2 \ln(d_{hb}) - 2d_{hb}^4 P_m^2 \ln(R_m^2 t P_c + d_{hb}^2 P_m) + 2d_{hb}^4 P_m^2 \ln(P_m) + 2P_m t R_m^2 d_{hb}^2 P_c), & K = 2, \\ &\frac{1}{2t_1^3 R_m^6 P_c^3} (-6d_{hb}^2 P_m (R_m^2 t_1 P_c + d_{hb}^2 P_m)^2 \ln(R_m^2 t_1 P_c + d_{hb}^2 P_m) + 6d_{hb}^2 P_m (R_m^2 t_1 P_c + d_{hb}^2 P_m)^2 \ln(P_m) \\ &\quad + 12d_{hb}^2 P_m (R_m^2 t_1 P_c + d_{hb}^2 P_m)^2 \ln(d_{hb}) + 2t_1^3 R_m^6 P_c^3 + 9P_m t_1^2 R_m^4 d_{hb}^2 P_c^2 + 6d_{hb}^4 P_c R_m^2 t_1 P_m^2), & K = 3, \end{aligned} \right. \quad (16)$$

$$\times \mathcal{MG} \left(\left[0, \left[1 + \frac{1}{2}K, \frac{1}{2}K + \frac{1}{2} \right], \left[1, \frac{1}{2}, 0 \right], \left[\cdot \right], \frac{d_{hb}^4 P_m}{P_c R_m^4 t_3} \right] \right). \quad (18)$$

where $\mathcal{MG}(\cdot)$ denotes the Meijer's G function [41].

B. SECOND-HOP (T_2)

The BS works in FD mode in this hop, where the BS receives a signal from the cluster-head and simultaneously transmits its signal to the CUE. Therefore, the received signal at the BS is given by

$$y_b = \frac{\sqrt{P_h} x_h h_{hb}}{d_{hb}^{\alpha/2}} + \sqrt{P_b} x_b h_{bb} + n_b, \quad (19)$$

where x_h and x_b are the transmitted signals from the cluster-head and BS, respectively, with $|x_h|^2 = |x_b|^2 = 1$. P_b and P_h are the transmit powers of the BS and cluster-head, respectively; n_b is the AWGN at the BS with zero mean and variance of σ_b^2 and h_{bb} is the self-interference (SI) channel for the BS. In the interference limited scenario, the instantaneous SIR at the BS can be obtained from (19) as:

$$\gamma_b = \frac{\frac{P_h |h_{hb}|^2}{d_{hb}^{\alpha}}}{P_b |h_{bb}|^2 + \sigma_b^2} \leq \frac{I_{th} \gamma_{hb}}{\gamma_{RSI}}, \quad (20)$$

where γ_{hb} and γ_{hc_j} are the channel gains between the cluster-head and BS and between the cluster-head and CUE_j , respectively, while γ_{RSI} is the Residual SI (RSI) gain after employing the SI cancellation scheme [42].

Likewise, the SIR at the BS for the second hop can be improved by the best CUE selection as:

$$\gamma_{T_2} = \max_{j \in \{1 \dots L\}} \left(\frac{I_{th} \gamma_{hc_j}}{\gamma_{RSI}} \right) = \frac{I_{th} \frac{|h_{hb}|^2}{\min_{j \in \{1 \dots L\}} (|h_{hc_j}|^2)}}{\gamma_{RSI}}. \quad (21)$$

For better exposition, we let $X_2 = \min_{j \in \{1 \dots L\}} (|h_{hc_j}|^2)$, $Y_2 = |h_{hb}|^2$ and $Z = \gamma_{RSI}$. The PDF of Y_2 is e^{-y_2} and the PDF of X_2 after the best CUE selection is $f_{X_2}(x_2) = L e^{-Lx_2}$.

Then, the CDF of $R = Y_2/X_2$ and its PDF can be derived as (22) and (23), respectively:

$$F_R(r) = \int_0^\infty \int_0^{rx_2} f_{Y_2}(y_2) f_{X_2}(x_2) dy_2 dx_2 \\ = \frac{r}{r+L}, \quad (22)$$

$$f_R(r) = \frac{1}{r+L} - \frac{r}{(r+L)^2}. \quad (23)$$

Next, the PDF of Z can be obtained as:

$$f_Z(z) = \frac{e^{-z/\lambda_{RSI}}}{\lambda_{RSI}}. \quad (24)$$

Finally, we let $T_2 = I_{th} \frac{R}{Z}$ where the PDF of R and Z are given in (23) and (24), respectively. Therefore, the final expression of $F_{\gamma_{T_2}}$ can be obtained from (23) and (24) as:

$$F_{\gamma_{T_2}}(t_2) = \int_0^\infty \int_0^{\frac{t_2 z}{I_{th}}} f_R(r) f_Z(z) dr dz$$

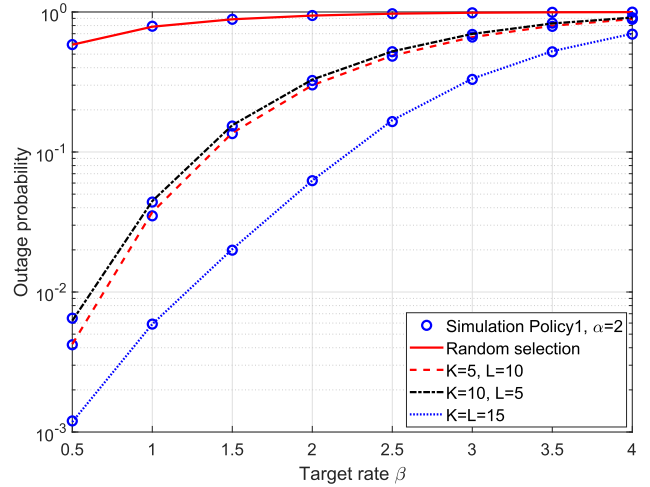


FIGURE 2. Numerical vs theoretical outage probability of policy 1 when $\alpha = 2$ with a different number of M2M and CUE devices, where $P_b = 5$ dB, $P_m = 10$ dB and $P_c = 30$ dB. $R_m = 15$ m, $R_c = 25$ m, $(X_h, Y_h) = (100, 100)$ m, and $I_{th} = 20$.

$$= 1 - \frac{I_{th} L e^{-\frac{I_{th} L}{t_2 \lambda_{RSI}}} \text{Ei}\left(1, \frac{I_{th} L}{t_2 \lambda_{RSI}}\right)}{t_2 \lambda_{RSI}}, \quad (25)$$

where $\text{Ei}(1, x)$ is the exponential integral function defined as: $\text{Ei}(1, x) = \int_1^\infty \frac{\exp(-tx)}{x} dt$, $x > 0$.

As DF relay is used at the cluster-head, the end-to-end SIR at the BS for M2M transmission can be written as:

$$\gamma_{end-end} = \min(\gamma_{T_1}^\Xi, \gamma_{T_2}), \quad (26)$$

where $\Xi \in \{\text{Policy1}, \text{Polic2}\}$. Then the CDF of $\gamma_{end-end}$ can be written as:

$$F_{\gamma_{end-end}}(\gamma) = 1 - (1 - F_{\gamma_{T_1}^\Xi}(\gamma))(1 - F_{\gamma_{T_2}}(\gamma)). \quad (27)$$

The outage probability is calculated when the SIR of the system is falling below a given threshold. Therefore, the outage probability of the proposed system can be obtained as

$$P_{out} = F_{\gamma_{end-end}}(b), \quad (28)$$

where $b = 2^{2\beta} - 1$ and β is the transmission rate in bits/s/Hz.

IV. SIMULATION RESULTS

In this section, we present the simulation results to verify our analysis. We assume that the noise variances σ_b^2 and σ_h^2 , are normalized to unity in our experiments. The analytical results based on (28) are presented here where the simulation results are obtained by averaging 10^6 independent Monte Carlo trials. In all cases, the simulation results match the analysis, which verifies the closed-form expressions for the outage probability derived in this paper.

Figs. 2 and 3 verify the outage probability expressions given in (28) for ordering policy 1 for different target rate values when $\alpha = 2$ and $\alpha = 4$, respectively. It can be observed from Fig. 2 and Fig. 3 that using our proposed joint selection scheme significantly decreases the outage probability. As a case in point, in Fig. 2 when the target transmission rate (β) = 1 bits/s/Hz, the outage probability with random

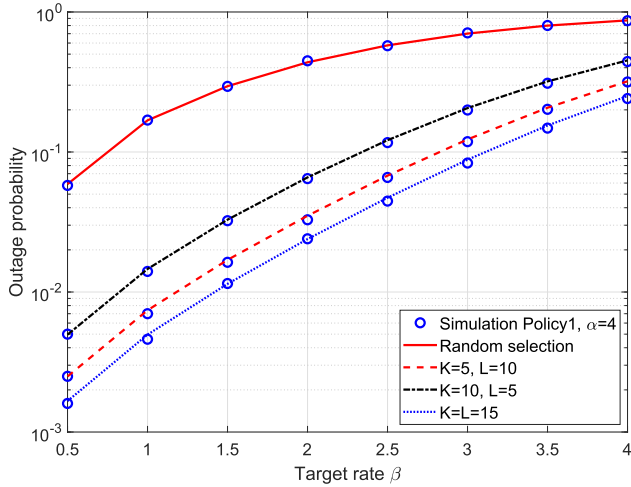


FIGURE 3. Numerical vs theoretical outage probability of policy 1 when $\alpha = 4$ with a different number of M2M and CUEs devices, where $P_b = 5$ dB, $P_m = 10$ dB, and $P_c = 40$ dB. $R_m = 15$ m, $R_c = 25$ m, $(X_h, Y_h) = (100, 100)$ m, and $I_{th} = 20$.

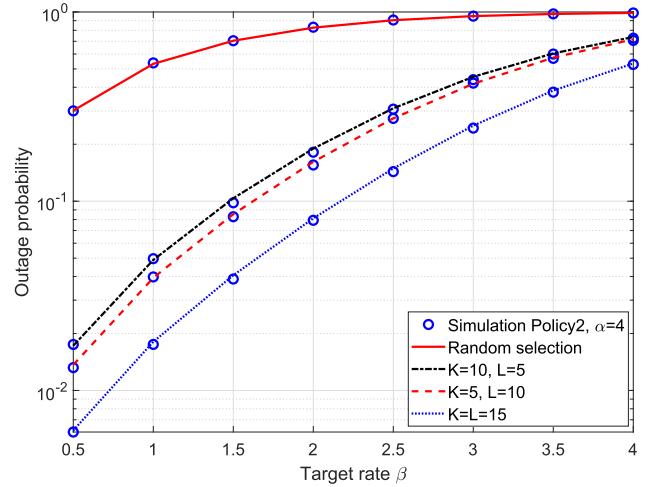


FIGURE 5. Numerical vs theoretical outage probability of policy 2 when $\alpha = 4$ with a different number of M2M and CUEs devices, where $P_b = 5$ dB, $P_m = 10$ dB, and $P_c = 40$ dB. $R_m = 15$ m, $R_c = 25$ m, $(X_h, Y_h) = (100, 100)$ m, and $I_{th} = 20$.

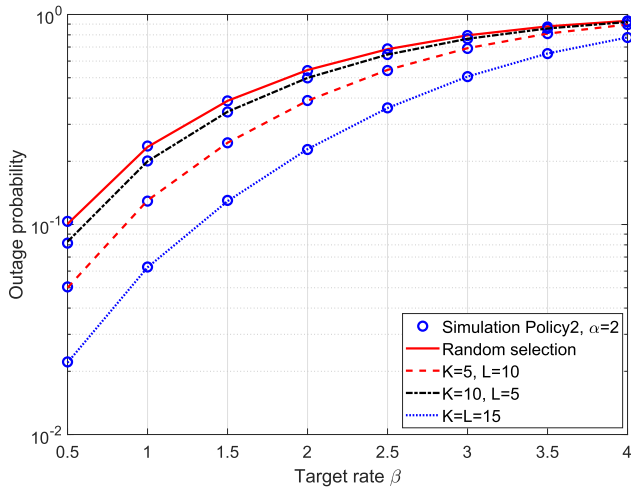


FIGURE 4. Numerical vs theoretical outage probability of policy 2 when $\alpha = 2$ with a different number of M2M and CUEs devices, where $P_b = 5$ dB, $P_m = 10$ dB, and $P_c = 40$ dB. $R_m = 15$ m, $R_c = 25$ m, $(X_h, Y_h) = (100, 100)$ m, and $I_{th} = 20$.

selection is approximately 0.8. However, a lower value equals to 3.7×10^{-2} for the outage probability is recorded when $K = 5, L = 10$. This value decreases further to 5.5×10^{-3} when $K = L = 15$. Similarly, in Fig. 3, when $\beta = 1$ bits/s/Hz, the outage probability with random selection is about 0.16, however, using the proposed scheme reduces the outage probability to 0.014 for $K = 5, L = 10$ and decreases it further to 0.0045 when $K = L = 15$.

On the other hand, Figs. 4 and 5 verify the outage probability expressions given in (28) for policy 2 with different target rates when $\alpha = 2$ and $\alpha = 4$, respectively. Again, the effect of the proposed selection scheme is clear in the aforementioned figures, where the outage probability is significantly reduced. For example in Fig. 4, when $\beta = 1$ bits/s/Hz, the outage probability with random selection is approximately 0.53. However, a lower value equals to 1.8×10^{-2} for the outage

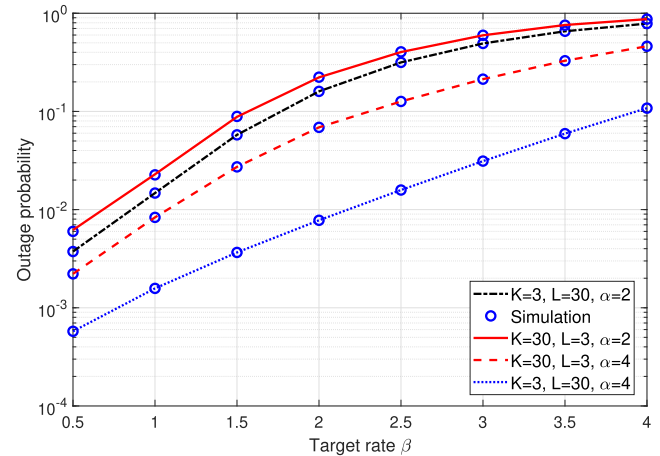


FIGURE 6. Comparison of outage probabilities of policy 1 for different number of M2M and CUEs devices with bigger gap where $P_b = 5$ dB, $P_m = 10$ dB, and $P_c = 40$ dB. $R_m = 15$ m, $R_c = 25$ m, $(X_h, Y_h) = (100, 100)$ m, and $I_{th} = 20$.

probability is recorded when $K = 5, L = 10$. This value decreases further to 3.9×10^{-2} when $K = L = 15$. In order to illustrate the effect of increasing the gap between the M2M and CUEs devices on the outage probability, Fig. 6 and Fig. 7 show the outage probability for different number of M2M and CUEs devices for policy 1 and policy 2, respectively, when $\alpha = 2$ and $\alpha = 4$.

Fig. 8 shows the outage probability versus different ordered M2M indices for policy 2. We can see that with increasing the order of indices (i.e., first, third, 10^{th} best M2M device and so on), the outage probability increases as well for both $\alpha = 2$ and $\alpha = 4$, as expected.

Since the radio transmissions always encounter a bandwidth constraint that limits the maximum SI cancellation [42], Fig. 9 illustrates how RSI affects the outage performance of the FD scheme. Fig. 9 also shows the outage probability vs RSI (γ_{RSI}) for HD and FD where γ_{RSI} is varied

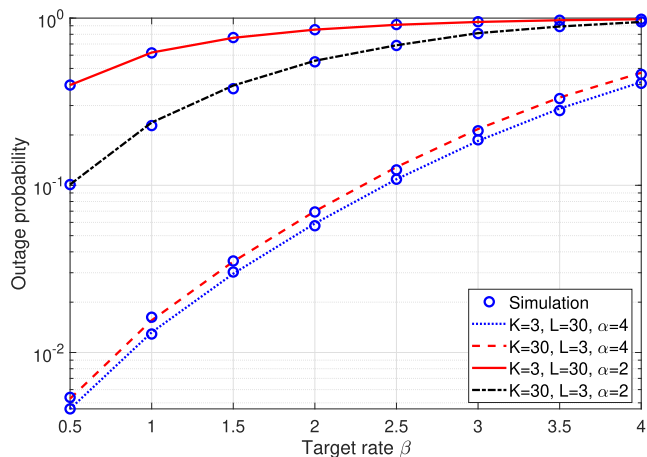


FIGURE 7. Comparison of outage probabilities of policy 2 for different number of M2M and CUE devices with bigger gap where $P_b = 5$ dB, $P_m = 10$ dB and $P_c = 40$ dB. $R_m = 15$ m, $R_c = 25$ m, $(X_h, Y_h) = (100, 100)$ m, and $I_{th} = 20$.

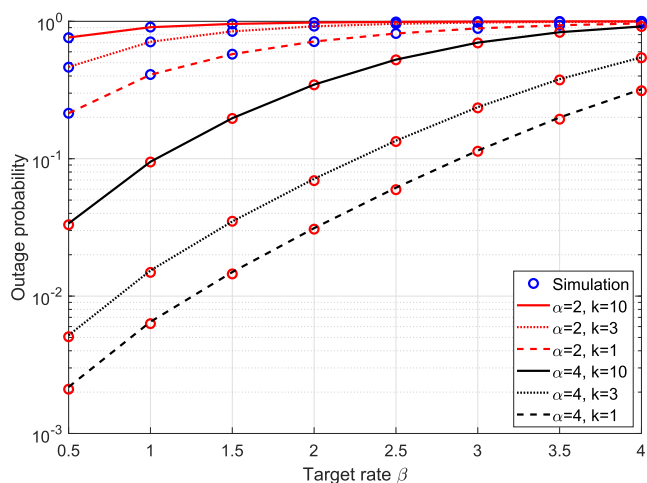


FIGURE 8. Comparison of outage probabilities for the different M2M ordinal indices where $K = L = 10$, $P_b = 5$ dB, $P_m = 10$ dB and $P_c = 40$ dB. $R_m = 15$ m, $R_c = 25$ m, $(X_h, Y_h) = (100, 100)$ m, and $I_{th} = 20$.

from 0 to 30 dB. It can be noticed that, when γ_{RSI} increases, the performance of the system becomes worse. Clearly, there is no SI for the HD scheme; therefore, the performance is constant for all γ_{RSI} in this figure. Of more interest is the observation that the outage probabilities for the HD mode are always higher than that related to the FD mode when γ_{RSI} is less than 11 dB and 17.5 dB when $\alpha = 4$ and $\alpha = 2$, respectively for policy 2. Similarly, the outage probabilities of the HD mode are always higher than the outage probabilities of the FD mode when γ_{RSI} is less than 10 dB for both values of α .

Moreover, it is clear from Fig. 9 that the outage probability of policy 1 is lower than that corresponding to policy 2. In practice, however, policy 1 requires knowledge of the instantaneous M2M to cluster-head channel gains, which cannot always be estimated accurately. On the other hand, policy 2 is dependent only on distance, or equivalently long-term average channel gains. Therefore, both policies are important in real life scenarios.

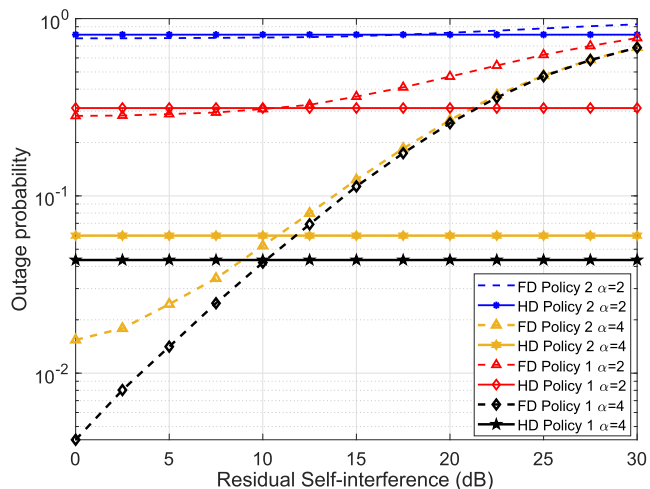


FIGURE 9. Outage probability vs residual self-interference (γ_{RSI}) corresponding to HD and FD modes for policy 1 and policy 2 when $\alpha = 2$ and $\alpha = 4$, where $I_{th} = 20$, $P_c = 35$ dB, $K = L = 10$, and $\beta = 1$ bits/s/Hz.

TABLE 2. Comparison of the time-slot for FD and HD.

Hops	Slots	Total slots
T_{1_HD}	1. $M2M_i \rightarrow cluster - head$	4
	2. $CUE_j \rightarrow BS$	
T_{2_HD}	1. $cluster - head \rightarrow BS$	3
	2. $BS \rightarrow CUE$	
T_{1_HD}	1. $M2M \rightarrow cluster - head$	3
	2. $BS \rightarrow CUE$	
T_{2_FD}	1. $cluster - head \rightarrow BS; BS \rightarrow CUE$	

Table 2 illustrates the effect of using FD in the second-hop (T_2). If the BS works in HD only, the total number of slots needed to complete the communication scheme would be 4, compared to only 3 slots for the proposed hybrid-duplex scheme. In addition, as the self-interference from BS is too strong for M2M communications when the BS works in FD mode, we therefore consider HD for the first hop.

The design of the proposed scheme takes into consideration that the machine devices are relatively simple and do not possess complicated processing capability, hence, there is no heavy computation associated with each M2M device. The cluster-head is responsible for performing the channel estimation and the selection of the machine device as well as the CUE. This operation has a low complexity of $\mathcal{O}(K + L)$, where $\mathcal{O}(\cdot)$ is the complexity order and K, L are the number of M2M and CUE devices, respectively. Similarly, this work adopts random selection as a reference scheme due to its low computational complexity [43], [44]. Detailed analysis of the complexity is beyond the scope of this work but interested readers can refer to [42], [45].

V. CONCLUSION

In this work, we proposed a cognitive cluster Machine-to-Machine (M2M) communications model with joint Cellular User Equipment (CUE) and M2M devices selection schemes to reduce the outage probability of M2M networks. Two ordering policies were proposed: the first one depends on average channel gain information from the M2M to the

cluster-head while the second one depends on instantaneous channel gains. The proposed schemes achieved a significant reduction in the outage probability for M2M networks as verified with the simulation results. Furthermore, a Hybrid-duplex BS was exploited to switch between Half-Duplex (HD) and Full-Duplex (FD) modes to attain the best performance corresponding to various levels of residual self-interference. The approximated closed-form formulas for the outage probability corresponding to each of the proposed ordering policies, and for different path loss exponents, were derived and verified through Monte Carlo simulations.

REFERENCES

- [1] L. Atzori, A. Iera, and G. Morabito, "The Internet of Things: A survey," *Comput. Netw.*, vol. 54, no. 15, pp. 2787–2805, Oct. 2010.
- [2] Y. Cao, T. Jiang, and Z. Han, "A survey of emerging M2M systems: Context, task, and objective," *IEEE Internet Things J.*, vol. 3, no. 6, pp. 1246–1258, Dec. 2016.
- [3] G. Chen, J. P. Coon, A. Mondal, B. Allen, and J. A. Chambers, "Performance analysis for multihop full-duplex IoT networks subject to Poisson distributed interferers," *IEEE Internet Things J.*, vol. 6, no. 2, pp. 3467–3479, Apr. 2019.
- [4] S. Chen, R. Ma, H.-H. Chen, H. Zhang, W. Meng, and J. Liu, "Machine-to-machine communications in ultra-dense networks—A survey," *IEEE Commun. Surveys Tuts.*, vol. 19, no. 3, pp. 1478–1503, 3rd Quart., 2017.
- [5] *More Than 50 Billion Connected Devices, White Paper*, Ericsson, Stockholm, Sweden, Feb. 2011.
- [6] E. Soltanmohammadi, K. Ghavami, and M. Naraghi-Pour, "A survey of traffic issues in machine-to-machine communications over LTE," *IEEE Internet Things J.*, vol. 3, no. 6, pp. 865–884, Dec. 2016.
- [7] G. Chen, J. Tang, and J. P. Coon, "Optimal routing for multihop social-based D2D communications in the Internet of Things," *IEEE Internet Things J.*, vol. 5, no. 3, pp. 1880–1889, Jun. 2018.
- [8] H.-K. Lee, D. M. Kim, Y. Hwang, S. M. Yu, and S.-L. Kim, "Feasibility of cognitive machine-to-machine communication using cellular bands," *IEEE Wireless Commun.*, vol. 20, no. 2, pp. 97–103, Apr. 2013.
- [9] W. Ejaz, N. Ul Hasan, and H. S. Kim, "Distributed cooperative spectrum sensing in cognitive radio for ad hoc networks," *Comput. Commun.*, vol. 36, no. 12, pp. 1341–1349, Jul. 2013.
- [10] X. Zhang, X. Zhang, L. Han, and R. Xing, "Utilization-oriented spectrum allocation in an underlay cognitive radio network," *IEEE Access*, vol. 6, pp. 12905–12912, Feb. 2018.
- [11] A. Asadi, Q. Wang, and V. Mancuso, "A survey on device-to-device communication in cellular networks," *IEEE Commun. Surveys Tuts.*, vol. 16, no. 4, pp. 1801–1819, 4th Quart., 2014.
- [12] G. Farhadi and A. Ito, "Group-based signaling and access control for cellular machine-to-machine communication," in *Proc. IEEE Veh. Technol. Conf.*, Las Vegas, NV, USA, Sep. 2013, pp. 1–6.
- [13] L. Liang, L. Xu, B. Cao, and Y. Jia, "A cluster-based congestion-mitigating access scheme for massive M2M communications in Internet of Things," *IEEE Internet Things J.*, vol. 5, no. 3, pp. 2200–2211, Jun. 2018.
- [14] S.-H. Wang, H.-J. Su, H.-Y. Hsieh, S.-P. Yeh, and M. Ho, "Random access design for clustered wireless machine to machine networks," in *Proc. 1st Int. Black Sea Conf. Commun. Netw. (BlackSeaCom)*, Batumi, Georgia, Jul. 2013, pp. 107–111.
- [15] K.-R. Jung, A. Park, and S. Lee, "Machine-type-communication (MTC) device grouping algorithm for congestion avoidance of MTC oriented LTE network," in *Security-Enriched Urban Computing and Smart Grid*, T.-H. Kim, A. Stoica, and R.-S. Chang, Eds. Berlin, Germany: Springer, 2010, pp. 167–178.
- [16] M. A. M. Abdullah, G. Chen, M. Alageli, A. Ikhlef, and J. Chambers, "Performance analysis of cognitive clustered machine-to-machine networks with device selection," in *Proc. IEEE Globecom Workshops (GC Wkshps)*, Dec. 2018, pp. 1–5.
- [17] M. Haenggi, J. G. Andrews, F. Baccelli, O. Dousse, and M. Franceschetti, "Stochastic geometry and random graphs for the analysis and design of wireless networks," *IEEE J. Sel. Areas Commun.*, vol. 27, no. 7, pp. 1029–1046, Sep. 2009.
- [18] G. Chen and J. P. Coon, "Secrecy outage analysis in random wireless networks with antenna selection and user ordering," *IEEE Wireless Commun. Lett.*, vol. 6, no. 3, pp. 334–337, Jun. 2017.
- [19] G. Chen, J. P. Coon, and M. Di Renzo, "Secrecy outage analysis for downlink transmissions in the presence of randomly located eavesdroppers," *IEEE Trans. Inf. Forensics Security*, vol. 12, no. 5, pp. 1195–1206, May 2017.
- [20] M. Afshang and H. S. Dhillon, "Fundamentals of modeling finite wireless networks using binomial point process," *IEEE Trans. Wireless Commun.*, vol. 16, no. 5, pp. 3355–3370, May 2017.
- [21] S. Srinivasa and M. Haenggi, "Distance distributions in finite uniformly random networks: Theory and applications," *IEEE Trans. Veh. Technol.*, vol. 59, no. 2, pp. 940–949, Feb. 2010.
- [22] S. Ilari, D. Stojanovic, and C. Ray, "Semantic management of moving objects: A vision towards smart mobility," *Expert Syst. Appl.*, vol. 42, no. 3, pp. 1418–1435, 2015.
- [23] R. Costa, "The Internet of moving things [industry view]," *IEEE Technol. Soc. Mag.*, vol. 37, no. 1, pp. 13–14, Mar. 2018.
- [24] H. ElSawy, E. Hossain, and M. Haenggi, "Stochastic geometry for modeling, analysis, and design of multi-tier and cognitive cellular wireless networks: A survey," *IEEE Commun. Surveys Tuts.*, vol. 15, no. 3, pp. 996–1019, 3rd Quart., 2013.
- [25] H. ElSawy, A. Sultan-Salem, M. S. Alouini, and M. Z. Win, "Modeling and analysis of cellular networks using stochastic geometry: A tutorial," *IEEE Commun. Surveys Tuts.*, vol. 19, no. 1, pp. 167–203, 1st Quart., 2017.
- [26] D. Malak, H. S. Dhillon, and J. G. Andrews, "Optimizing data aggregation for uplink machine-to-machine communication networks," *IEEE Trans. Commun.*, vol. 64, no. 3, pp. 1274–1290, Mar. 2016.
- [27] N. Kouzayha, Z. Dawy, and J. G. Andrews, "Analysis of a power efficient wake-up solution for M2M over cellular using stochastic geometry," in *Proc. IEEE Global Commun. Conf. (GLOBECOM)*, Dec. 2016, pp. 1–7.
- [28] S. N. Swain, R. Thakur, and S. R. M. Chebiyyam, "Coverage and rate analysis for facilitating machine-to-machine communication in LTE-A networks using device-to-device communication," *IEEE Trans. Mobile Comput.*, vol. 16, no. 11, pp. 3014–3027, Nov. 2017.
- [29] G. Chen, Z. Tian, Y. Gong, and J. Chambers, "Decode-and-forward buffer-aided relay selection in cognitive relay networks," *IEEE Trans. Veh. Technol.*, vol. 63, no. 9, pp. 4723–4728, Nov. 2014.
- [30] S. Dang, J. P. Coon, and G. Chen, "An equivalence principle for OFDM-based combined bulk/per-subcarrier relay selection over equally spatially correlated channels," *IEEE Trans. Veh. Technol.*, vol. 66, no. 1, pp. 122–133, Jan. 2017.
- [31] G. Chen and J. A. Chambers, "Exact outage probability analysis for cooperative AF relay network with relay selection in presence of inter-cell interference," *Electron. Lett.*, vol. 48, no. 21, pp. 1346–1347, Oct. 2012.
- [32] A. Ghasemi and E. S. Sousa, "Fundamental limits of spectrum-sharing in fading environment," *IEEE Trans. Wireless Commun.*, vol. 6, no. 2, pp. 649–658, Feb. 2007.
- [33] K. Hamdi, W. Zhang, and K. B. Letaief, "Power control in cognitive radio systems based on spectrum sensing side information," in *Proc. IEEE Int. Conf. Commun., Glasgow, U.K.*, Jun. 2007, pp. 5161–5165.
- [34] J. Dai and S. Wang, "Clustering-based interference management in densely deployed femtocell networks," *Digit. Commun. Netw.*, vol. 2, no. 4, pp. 175–183, 2016.
- [35] M. Haenggi and R. K. Ganti, "Interference in large wireless networks," *Found. Trends Netw.*, vol. 3, no. 2, pp. 127–248, 2009.
- [36] I. S. Gradshteyn and I. M. Ryzhik, *Table of Integrals, Series, and Products*, 7th ed. Amsterdam, The Netherlands: Elsevier, 2007.
- [37] S. Dang, G. Chen, and J. P. Coon, "Multicarrier relay selection for full-duplex relay-assisted OFDM D2D systems," *IEEE Trans. Veh. Technol.*, vol. 67, no. 8, pp. 7204–7218, Aug. 2018.
- [38] W.-J. Tsay, C. J. Huang, T.-T. Fu, and I.-L. Ho, "A simple closed-form approximation for the cumulative distribution function of the composite error of stochastic frontier models," *J. Productiv. Anal.*, vol. 39, no. 3, pp. 259–269, Jun. 2013.
- [39] S. Dang, J. P. Coon, and G. Chen, "Outage performance of two-hop OFDM systems with spatially random decode-and-forward relays," *IEEE Access*, vol. 5, pp. 27514–27524, 2017.
- [40] F. W. Olver, D. W. Lozier, R. F. Boisvert, and C. W. Clark, *NIST Handbook of Mathematical Functions*, 1st ed. New York, NY, USA: Cambridge Univ. Press, 2010.

- [41] M. Abramowitz and I. A. Stegun, *Handbook of Mathematical Functions, With Formulas, Graphs, and Mathematical Tables*. New York, NY, USA: Dover, 1965.
- [42] M. Jain, J. Choi, T. M. Kim, D. Bharadia, S. Seth, K. Srinivasan, P. Levis, S. Katti, and P. Sinha, "Practical, real-time, full duplex wireless," in *Proc. 17th Annu. Int. Conf. Mobile Comput. Netw. (MobiCom)*, New York, NY, USA, Sep. 2011, pp. 301–312.
- [43] L. P. Qian, Y. Wu, J. Wang, and W. Zhang, "Energy-efficient distributed user scheduling in relay-assisted cellular networks," *IEEE Trans. Wireless Commun.*, vol. 15, no. 6, pp. 4060–4073, Jun. 2016.
- [44] J. Cui, Y. Liu, Z. Ding, P. Fan, and A. Nallanathan, "Optimal user scheduling and power allocation for millimeter wave NOMA systems," *IEEE Trans. Wireless Commun.*, vol. 17, no. 3, pp. 1502–1517, Mar. 2018.
- [45] B. Debaillie, D.-J. van den Broek, C. Lavín, B. van Liempd, E. A. M. Klumperink, C. Palacios, J. Craninckx, B. Nauta, and A. Pärssinen, "Analog/RF solutions enabling compact full-duplex radios," *IEEE J. Sel. Areas Commun.*, vol. 32, no. 9, pp. 1662–1673, Sep. 2014.



MOHAMMED A. M. ABDULLAH (M'10) received the B.Sc. and M.Sc. degrees in computer engineering from Iraq, in 2008 and 2010, respectively, and the Ph.D. degree from the School of Electrical and Electronic Engineering, Newcastle University, U.K., in 2017. Since 2017, he has been a Research Fellow of the Department of Computer Science, University of St Andrews. He was a Postdoctoral Researcher with the Department of Engineering, The University of Leicester, U.K. He is currently a Lecturer with the Department of Computer Engineering, Ninevah University. His research interests include the fields of pattern recognition, machine learning, signal processing, and wireless communication. He is a member of the International Biometric Society (IBS) and the British Machine Vision Association (BMVA). He is also an Associate Fellow of the U.K. Higher Education Academy (AFHEA).



ZAID ABDULLAH (M'18) received the B.Sc. degree in electrical engineering (electronics and communications) from Mosul University, Mosul, Iraq, in 2012, and the M.Sc. and Ph.D. degrees in communications and signal processing from Newcastle University, U.K., in 2014 and 2019, respectively. He is currently a Postdoctoral Research Assistant with the Digital Communications and Intelligent Sensing Group, Department of Engineering, University of Leicester, U.K. His main research interests include Massive MIMO systems, M2M, NOMA, and low-complexity algorithms design.



GAOJIE CHEN (S'09–M'12–SM'18) received the B.Eng. degree in electrical information engineering and the B.Ec. degree in international economics and trade from Northwest University, China, in 2006, and the M.Sc. (Hons.) and Ph.D. degrees in electrical and electronic engineering from Loughborough University, Loughborough, U.K., in 2008 and 2012, respectively. From 2008 to 2009, he was a Software Engineering with DTmobile, Beijing, China, and from 2012 to 2013, he was a Research Associate with the School of Electronic, Electrical and Systems Engineering, Loughborough University. He was a Research Fellow of 5GIC, Faculty of Engineering and Physical Sciences, University of Surrey, U.K., from 2014 to 2015. Then, he was a Research Associate with the Department of Engineering Science, University of Oxford, U.K., from 2015 to 2018. He is currently a Lecturer with the Department of Engineering, University of Leicester, U.K. His current research interests include information theory, wireless communications, cooperative communications, cognitive radio, secrecy communication, and random geometric networks. He received the Exemplary Reviewer Certificate for the IEEE WIRELESS COMMUNICATION LETTERS, in 2018. He has been served as an Editor for *IET Electronics Letters*, since 2018.



JIE TANG (S'10–M'13–SM'18) received the B.Eng. degree in information engineering from the South China University of Technology, Guangzhou, China, in 2008, the M.Sc. degree (Hons.) in communication systems and signal processing from the University of Bristol, U.K., in 2009, and the Ph.D. degree from Loughborough University, Loughborough, U.K., in 2012.

He held a Postdoctoral Research positions at the School of Electrical and Electronic Engineering, The University of Manchester, U.K. He is currently an Associate Professor with the School of Electronic and Information Engineering, South China University of Technology. His research interests include green communications, NOMA, 5G networks, simultaneous wireless information and power transfer, heterogeneous networks, cognitive radio, and device-to-device communications. He was a co-recipient of the 2018 IEEE ICNC Best Paper Award. He has served as the Track Co-Chair for the IEEE Vehicular Technology Conference, in 2018. He currently serves as an Editor for IEEE Access, the *EURASIP Journal on Wireless Communications and Networking*, *Physical Communication*, and *Ad Hoc & Sensor Wireless Networks*.



JONATHON CHAMBERS (S'83–M'90–SM'98–F'11) received the Ph.D. and D.Sc. degrees in signal processing from Imperial College London, London, U.K., in 1990 and 2014, respectively.

From 1991 to 1994, he was a Research Scientist with the Schlumberger Cambridge Research Center, Cambridge, U.K. In 1994, he returned to Imperial College London as a Lecturer in signal processing, and he was promoted to a Reader (Associate Professor), in 1998. From 2001 to 2004, he was the Director of the Center for Digital Signal Processing and a Professor of signal processing with the Division of Engineering, King's College London, where he is currently a Visiting Professor. From 2004 to 2007, he was a Cardiff Professorial Research Fellow of the School of Engineering, Cardiff University, Cardiff, U.K. From 2007 to 2014, he led the Advanced Signal Processing Group, School of Electronic, Electrical and Systems Engineering, Loughborough University, where he was also a Visiting Professor. In 2015, he joined the School of Electrical and Electronic Engineering, Newcastle University, Newcastle upon Tyne, U.K., where he has been with the School of Engineering, since 2017. Since 2017, he has also been a Professor in engineering and the Head of the Department, University of Leicester, Leicester, U.K. He is also the International Honorary Dean and a Guest Professor with the Department of Automation, Harbin Engineering University, Harbin, China. He has advised almost 80 researchers through to Ph.D. graduation. He has published over 500 conference proceedings and journal articles, many of which are in IEEE journals. His research interests include adaptive signal processing, and machine learning and their applications in communications, defense, and navigation systems. He is a Fellow of the Royal Academy of Engineering, U.K., the Institution of Engineering and Technology, and the Institute of Mathematics and its Applications. He was the Technical Program Co-Chair of the 36th IEEE International Conference on Acoustics, Speech, and Signal Processing (ICASSP), Prague, Czech Republic. He is serving on the Organizing Committees of ICASSP 2019, Brighton, U.K., and ICASSP 2022, Singapore. He has served on the IEEE Signal Processing Theory and Methods Technical Committee for six years, the IEEE Signal Processing Society Awards Board for three years, and the Jack Kilby Medal Committee for three years. He was an Associate Editor of the IEEE TRANSACTIONS ON SIGNAL PROCESSING for three terms, from 1997 to 1999 and from 2004 to 2007, and a Senior Area Editor, from 2011 to 2015.

...